ADVANCED MATERIALS

the air hole array of a triangular lattice in an alumina matrix. For the formation of a fluorescent-dye layer on the surface of porous alumina, the porous alumina substrate was dipped in an ethanol solution containing 20 wt.-% dendrimer [13] and 4×10^{-3} M pyrromethene 597 (EXITON) for 1 min and then dried. The thickness of the fluorescent-dye layer was approximately 1 μm.

Optically pumped lasing experiments were performed using a frequency doubled Nd^{3+}:yttrium aluminum garnet (YAG) pulse laser (532 nm wavelength, 8 ns pulse width, and 10 Hz repetition rate). The spot size of the incident light was 300 μm. The excitation light from the laser was irradiated from a direction parallel to the cylinder array to the surface of the fluorescent-dye layer. The emission from the cross section of porous alumina cut in the *Γ*–*X* direction was observed using a spectrometer.

Received: November 27, 2004
Final version: June 30, 2005
Published online: December 5, 2005

[1] E. Yablonovitch, T. J. Gmitter, *Phys. Rev. Lett.* **1989**, *63*, 1950.
[2] J. D. Jonnopoulso, R. D. Meade, J. N. Winn, *Photonic Crystals*, Princeton University Press, Princeton, NJ **1995**.
[3] K. Inoue, M. Sakoda, J. Kawamata, K. Sakoda, J. W. Haus, *Jpn. J. Appl. Phys., Part 2* **1999**, *38*, L157.
[4] M. Meier, A. Mekis, A. Dodabalapur, A. Timko, R. E. Slusher, J. D. Joannopoulos, O. Nalamasu, *Appl. Phys. Lett.* **1999**, *74*, 7.
[5] M. Notomi, H. Suzuki, T. Tamamura, *Appl. Phys. Lett.* **2001**, *78*, 1325.
[6] S. Riechel, C. Kallinger, U. Lemmer, J. Feldmann, A. Gombert, V. Witter, U. Scherf, *Appl. Phys. Lett.* **2000**, *77*, 23 210.
[7] V. I. Kopp, A. Z. Genack, Z.-Q. Zhang, *Phys. Rev. Lett.* **2001**, *86*, 1753.
[8] J. R. Lawrence, G. A. Turnbull, I. D. W. Samuel, *Appl. Phys. Lett.* **2003**, *82*, 4023.
[9] A. Jebali, R. F. Mahrt, N. Moll, D. Erni, C. Bauer, G.-L. Bona, W. Bachtold, *J. Appl. Phys.* **2004**, *96*, 3043.
[10] H. Masuda, M. Ohya, H. Asoh, M. Nakao, M. Nohtomi, T. Tamamura, *Jpn. J. Appl. Phys., Part 2* **1999**, *38*, L1403.
[11] H. Masuda, M. Ohya, K. Nishio, H. Asoh, N. Nakao, M. Nohtomi, A. Yokoo, T. Tamamura, *Jpn. J. Appl. Phys., Part 2* **2000**, *39*, L1039.
[12] H. Masuda, M. Ohya, H. Asoh, K. Nishio, *Jpn. J. Appl. Phys., Part 2* **2001**, *40*, L1217.
[13] S. Yokoyama, A. Otomo, S. Mashiko, *Appl. Phys. Lett.* **2002**, *80*, 7.
[14] A. Otomo, S. Otomo, S. Yokoyama, S. Mashiko, *Opt. Lett.* **2002**, *27*, 891.

DOI: 10.1002/adma.200501716

Direction-Dependent Homoepitaxial Growth of GaN Nanowires**

By *Hongwei Li*, *Alan H. Chin*, and *Mahendra K. Sunkara**

Wurtzite GaN is a technologically important material for optoelectronics and has potential applications in high-temperature and high-power electronics.[1–3] One-dimensional (1D) structures have attracted great interest as potential building blocks for nanoscale electronics.[4,5] Due to its anisotropic and polar nature, GaN exhibits direction-dependent properties.[6,7] Thus, controlling the growth direction of GaN nanowires is important for practical applications. In addition, it is important to be able to obtain these nanowires in a wide range of sizes, from micrometers to nanometers, for easier optical and electrical coupling. Up until now, wurtzite GaN nanowires have been primarily synthesized using either catalyst-mediated or oxide-assisted techniques,[8,9] or through direct-nitridation schemes.[10] Recently, control of the growth direction of GaN nanowires has been achieved using heteroepitaxy on different single-crystal templates, mediated by catalyst clusters;[8] however, control of the growth direction is yet to be achieved for nanowires grown by direct-nitridation methods. Moreover, there is no procedure available to statistically evaluate the growth directions of all the nanowires in a sample. Specifically, nanowires with diameters less than 30 nm do not show clear facets and appear rounded under observation by field-emission scanning electron microscopy (FESEM). Here, we report a direct-nitridation scheme for the controllable synthesis of GaN nanowires in two distinct directions (<0001> *c*-direction and <10–10> *a*-direction) using amorphous substrates and describe a simple procedure based on homoepitaxy to determine the growth directions of the resulting nanowires. Homoepitaxy onto wires grown in the *c*-direction results in hexagonal microprismatic island growth at the ends, which could possibly be exploited for optical and electrical coupling.

[*] Prof. M. K. Sunkara, H. Li
Department of Chemical Engineering, University of Louisville
106 Ernst Hall, Louisville, KY 40292 (USA)
E-mail: mahendra@louisville.edu
Dr. A. H. Chin
ELORET Corporation, NASA Ames Research Center
M/S N229-1, Moffett Field, CA 94035 (USA)

[**] This work was supported by U.S. Air Force Research (AFOSR, F49620-00-1-0310, monitored by Dr. Gerald Witt), U.S. National Science Foundation (CTS 9 876 251), and the Kentucky Science & Engineering Foundation (KSEF-148-502-04-86). The authors acknowledge Dr. Xu at the University of Kentucky for help with HRTEM and Dr. Raul Miranda of the Basic Energy Sciences Division at the U.S. Department of Energy for helpful discussions. Supporting Information is available online from Wiley InterScience or from the author.

Homoepitaxy onto wires grown in the *a*-direction leads to uniform growth over the entire length of the wires and results in the formation of thin, two-dimensional (2D) microbelts. The morphological features observed upon homoepitaxy onto wires grown in the *c*-direction suggest a "ballistic" or 1D transport mechanism, as compared to the traditional "slow" diffusion of adatoms on the surfaces of wires grown in the *a*-direction.

In this study, control over the growth direction of the resulting nanowires has been obtained by controlling the Ga flux during direct nitridation in dissociated ammonia. The nitridation of Ga droplets at a high flux leads to GaN nanowire growth in the *c*-direction (<0001>), while nitridation with a low Ga flux leads to growth in the *a*-direction (<10–10>). Micrographs, including lattice images of GaN nanowires grown in the two different directions (*c*- and *a*-directions), are shown in Figure 1. The inset of Figure 1a shows GaN nanowire growth from Ga droplets, as is typically observed on spontaneous nucleation followed by basal growth, similar to the phenomena observed in our previous studies of bulk Si nanowire growth using molten Ga pools.[11] In this case, the nanowires are expected to grow in the *c*-direction due to the expected alignment of the basal (0001) planes of the GaN crystal nuclei with the molten Ga surface.[12] The presence of hydrogen in the gas phase during growth reduces the wettability of GaN with Ga, thereby restricting the lateral propagation of the nuclei and leading to 1D growth. The diameters of the nanowires range from 15 to 40 nm, with an average diameter of 20 nm, and the lengths can be as much as 100 μm (Fig. 1a). High-resolution transmission electron microscopy (HRTEM) analysis of nanowires grown in the *c*-direction shows a regular occurrence of stacking errors along the *c*-direction, but no amorphous oxide sheath is observed on the surfaces (Fig. 1b).

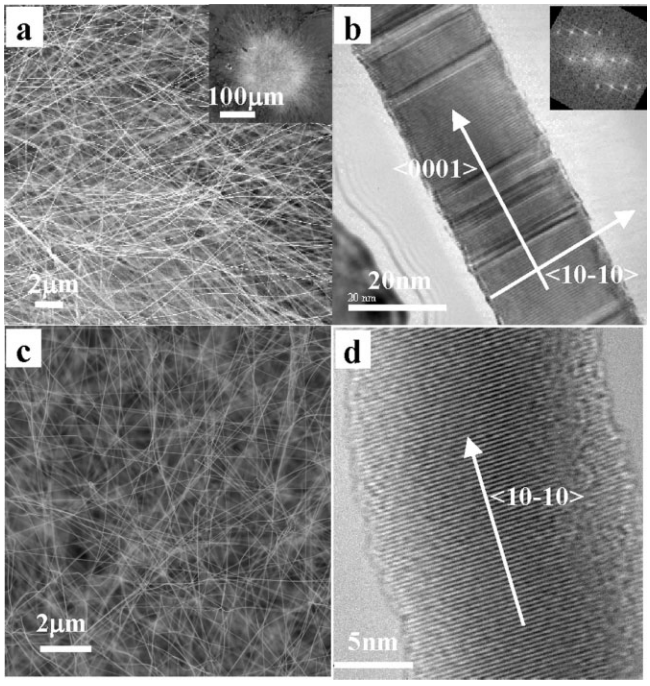

Figure 1. a) SEM images showing GaN nanowires with diameters less than 30 nm obtained from the direct reaction of Ga droplets and NH_3. The inset shows the spontaneous nucleation and growth of multiple nanowires directly from a larger Ga droplet. b) High-resolution transmission electron microscopy (HRTEM) image of a GaN nanowire from the sample shown in (a) indicating that the growth direction is <0001>. The inset is a fast Fourier transform of the HRTEM image, and the zone axis is <11–20>. c) SEM image showing GaN nanowires with diameters less than 30 nm resulting from the reactive-vapor transport of a controlled Ga flux in a NH_3 atmosphere. d) TEM image of a GaN nanowire from the sample shown in (c) indicating that the growth direction is <10–10>.

GaN nanowires grown in the *a*-direction have been obtained from experiments utilizing the controlled vapor transport of Ga (or a low Ga flux using pre-synthesized polycrystalline GaN as the Ga source) in the presence of dissociated ammonia on quartz substrates (Figs. 1c,d). These experiments are similar to our recent work on the vapor-transport synthesis of InN nanowires using indium and ammonia.[13] That study showed that InN crystal nucleation occurs first, and is followed subsequently by 1D growth by liquid-phase epitaxy through the In droplets in a tip-led fashion. The Ga droplets at the tips of long and thin nanowires may possibly evaporate after growth, and have not been observed in our experiments. TEM analysis (Fig. 1d) of the nanowires shows that they are free from stacking faults and dislocations and contain no amorphous oxide sheath.

The bandgap of wurtzite GaN has been found to be dependent on the crystallographic orientation because of polarization in the *c*-direction of GaN crystals.[7] This is illustrated by the blue-shift in the bandgap of GaN nanowires grown in the *a*-direction by about 100 meV, as compared to wires grown in the *c*-direction, at temperatures ranging from 0–300 K.[8] Here, photoluminescence (PL) data has been obtained at different laser irradiation powers for samples containing GaN nanowires with diameters less than 30 nm grown in both *c*- and *a*-directions. The samples are excited using a 325 nm He–Cd continuous wave (CW) UV laser. Broad peaks centered around 3.1 eV to 3.5 eV are observed at different laser powers, and these peaks exhibit red-shifts with increasing laser power (see Supporting Information). A spectral dip is also apparent at around 3.4 eV. Laser-induced heating likely occurs in the nanowires due to the small spot size involved (~ 10 μm × 10 μm), resulting in decreased bandgap values for GaN.[14] The bandgap variation with temperature *E(T)* for GaN follows the Varshini formula,[15]

$$E(T) = E_0 - aT^2/(T+b) \quad (1)$$

where E_0 is the bandgap of GaN at 0 K, and *a* and *b* are Varshini's fitting parameters. The spectral dip is likely due to the spectral response of the PL system used here. By assuming a Gaussian shape for the spectral dip, and correcting and fitting the spectra to obtain the PL peak values, the bandgap of these nanowires has been correlated to the laser intensity, as shown in Figure 2. The bandgap of the wires grown in the *a*-direction blue-shifts by about 50 meV compared to nanowires grown in the *c*-direction, which is less of an effect than

ADVANCED MATERIALS

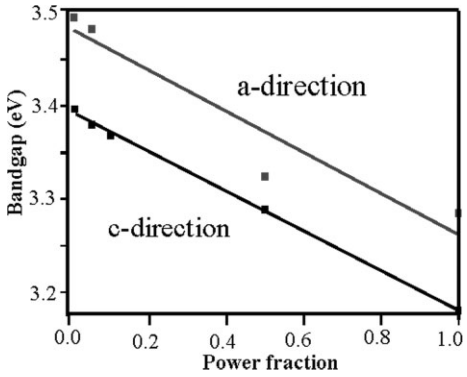

Figure 2. The plot shows the bandgap values estimated from the PL data for GaN nanowires grown in both *a*- and *c*-directions as a function of the incident laser intensity. Full power of the laser irradiation used was 17 mW.

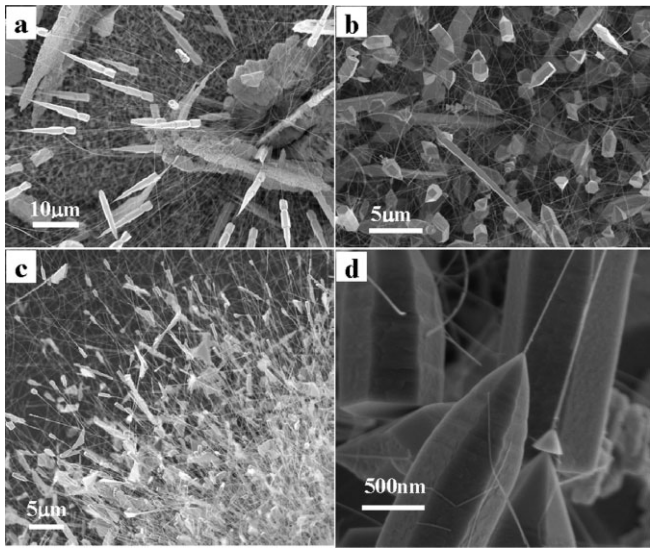

Figure 3. a–d) SEM images showing the morphologies resulting from homoepitaxial-growth experiments on several GaN nanowire samples grown along the *c*-direction. The images show hexagonal-island growth at the ends of the wires or at several places on the wires, with the separation between the islands being several tens of micrometers.

previously reported.[8] The reasons for this are not completely clear, but could be due to the differences in the surface facets of the wires and the actual temperature to which the nanowires are heated by the laser.

There is no reliable procedure for evaluating the growth directions of large quantities of nanowires. Such a process is critical for controllably growing nanowires in specific directions. Here, homoepitaxy and analysis of the resulting morphological features by SEM is shown to be a simple process for determining the growth direction of GaN nanowires. The homoepitaxially grown morphological features clearly illustrate distinct differences depending upon the growth direction of the GaN nanowires: hexagonal prism-like island growth is observed for wires grown in the *c*-direction, while belt-shaped growth is observed for wires grown in the *a*-direction.

Most interestingly, the differences in the morphologies observed after homoepitaxy onto wires grown in different directions also reveal an interesting phenomenon, the enhanced surface diffusion of adatoms. Nanowires grown in the *c*-direction develop hexagonal island-shaped morphologies after homoepitaxy, as shown in Figure 3. The side surfaces of the observed hexagonal prisms belong to the {10–10} and {10–11} families of wurtzite GaN. The side planes of the top pyramids are {10–11}, since the ratio of their height to their base is about 0.85, close to the lattice ratio of $c/2a$ for wurtzite GaN. The {10–11} surfaces of the hexagonal prisms clearly show growth steps evolving from the pyramid tip to the hexagonal column, as illustrated in Figure 4a. The steps are seen to originate at the tip and propagate along the pyramid towards the hexagonal column. This clearly indicates that adatoms adsorbed on any part of the nanowire are transported to the hexagonal pyramids, where the steps are generated, followed by propagation towards the hexagonal ends, thereby extending the hexagonal column (Fig. 4b). Excluding the islands, the remaining portions of the nanowires do not grow in thickness during homoepitaxy. When multiple islands are present, the distances between islands grown on the same nanowire exceed several tens of micrometers, suggesting that

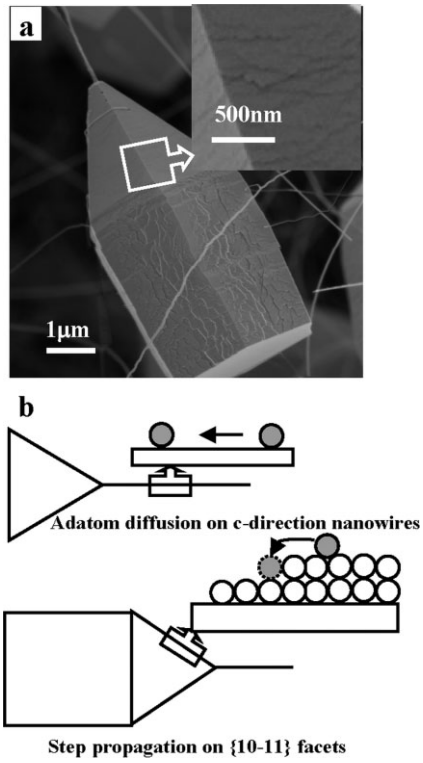

Figure 4. a) Enlarged SEM images of the {10–11} pyramidal side facets of the hexagonal islands grown on *c*-direction GaN nanowires, clearly indicating the step flow from the nanowires onto the hexagonal prisms. b) Schematic illustrating the adatom diffusion processes in the nanowire portion and on the {10–11} side facet, indicating the required adatom jump across the step.

the surface transport (diffusion) lengths of adatoms in GaN nanowires grown in the *c*-direction exceeds several tens of micrometers. The large surface diffusion lengths observed in these nanowires suggests "ballistic" or 1D type diffusion processes.

Homoepitaxial growth onto GaN nanowires grown in the *a*-direction leads to the belt-shaped morphologies shown in Figure 5a. The FESEM image of a resulting microbelt in Figure 5b clearly indicates preferential growth on one side of the nanowire. A TEM image of a 100 nm wide belt is shown in Figure 5c. One side of the belt is smooth while the other

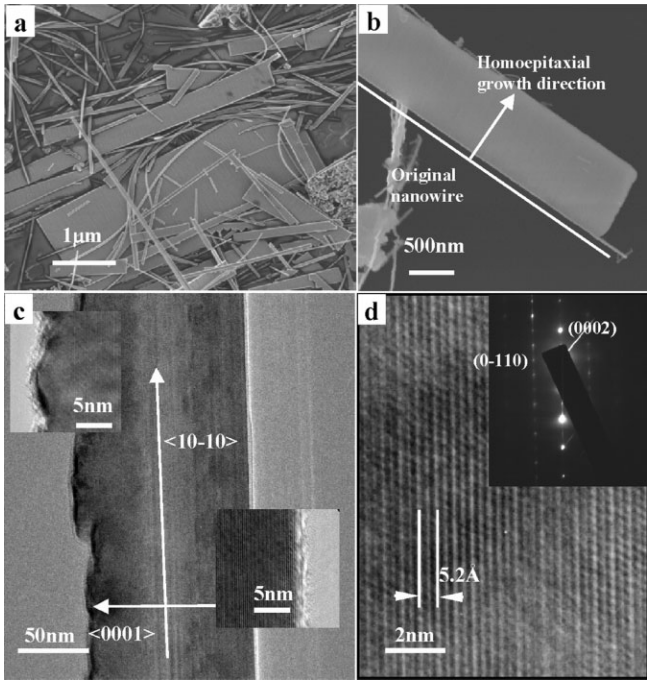

Figure 5. a) SEM image showing the belt-shaped morphology resulting from homoepitaxial growth onto GaN nanowires grown along the *a*-direction. b) SEM image of a 900 nm microbelt indicating preferential growth on one edge of the nanowire grown in the *a*-direction. c) TEM micrograph of 100 nm wide belts grown from *a*-direction GaN nanowires, along with two enlarged views of the edges, indicating Ga-terminated (right inset) and N-terminated (left inset) surfaces. d) Selected-area electron diffraction pattern with a <11–20> zone axis and a HRTEM image of the belt shown in (c), indicating that the direction perpendicular to the nanowire growth is <0001>.

side is rough. The direction perpendicular to the growth direction is determined to be <0001>, both from the selected-area electron diffraction (SAED) pattern and from the lattice spacing shown in Figure 5d. The large top surface of these microbelts is a (0–110) plane, and Raman spectra obtained for these microbelts show only the E_1 transverse optical (TO) peak, further corroborating the above conclusion (Supporting Information). We propose that the smooth side is the Ga-terminated surface and the rough side is the N-terminated surface (insets to Fig. 5c). Homoepitaxy on GaN nanowires grown in the *a*-direction results in preferential growth on the chemically active Ga-terminated surface, while no growth occurs on the other side (nitrogen terminated). The dependence of growth rates on the surface polarity of polar crystals has been reported previously for GaN and ZnS.[16,17] However, the above homoepitaxy experiments have been conducted using a low flux of Ga vapor. Increasing the Ga vapor flux could change the growth kinetics for preferential growth from the <0001> to the <11–20> direction, which will lead to the resulting belts being terminated by polar surfaces (0001).[18] Nevertheless, the results presented here establish a clear connection between the nanowire formation mechanism and the subsequent evolution of the nanowires to belt-like morphologies. The defect-free and uniform evolution of wires grown in the *a*-direction into 2D surfaces suggests that these nanowires could potentially serve as seeds for growing large GaN crystals. Ribbon- or belt-like morphologies have been reported previously[19] and have also been observed for polar materials such as GaN[20] and ZnO.[21] The mechanism proposed here should be universally applicable.

The observed "ballistic" surface diffusion phenomenon is found to be more specific to the side surfaces of wires grown along the *c*-direction, as compared to wires grown in the *a*-direction. The origin of this direction-dependent surface diffusion process can likely be traced to the "wettability" of polar versus non-polar surfaces during growth. The mean surface diffusion lengths of Ga on 2D surfaces under metal–organic chemical vapor deposition (MOCVD) growth conditions has been estimated to be on the order of 10–100 nm at 1050 °C, according to the lattice incorporation model.[22] Recently, Jensen et al.[23] reported that the surface diffusion length of In on 40–170 nm InAs nanowires is greater than 10 μm, and they also inferred from experiments with differently spaced nanowires that the diffusion length decreases with increasing wire diameter. Most relevantly, other studies have shown that the presence of two atomic layers of In or Ga enhances the surface transport of adatoms on GaN surfaces.[24] The side surfaces of the wires grown along the *c*-direction are all non-polar {10–10}, while the nanowires grown in the *a*-direction contain two polar surfaces ((0001) and (000–1)). The differences in the surface diffusion lengths for nanowires grown in the *c*- and *a*-directions can be attributed to differences in the adsorption of Ga on polar and non-polar surfaces. The observed uniform growth during homoepitaxy on nanowires grown in the *a*-direction indicates a lack of Ga adsorption on the polar surface. Also, this result is consistent with our proposed mechanism for the formation of nanowires along the *a*-direction by reactive-vapor transport, i.e., the selective wetting of Ga droplets on the non-polar surfaces of GaN crystals leads to nanowire growth along non-polar directions.

Homoepitaxy onto GaN nanowires with different growth directions also illustrates a simple analytical procedure for determining the growth direction of polar materials. As seen in Figures 1a,c, GaN nanowires with diameters less than 30 nm, grown along the *a*- and *c*-directions, both seem rod-like from SEM observations. However, homoepitaxial growth onto the different directional nanowires yields a dramatic contrast be-

ADVANCED MATERIALS

tween the morphologies: hexagonal-shaped microcrystals for the <0001> nanowires and flat, rectangular-shaped microbelts for nanowires grown along the <10–10> direction. These results are directly applicable to several other related material systems, both in terms of nanowire synthesis in different directions, as well as for synthesizing nanowires with macroscopic crystal attachments at their ends for optical coupling and contacts.

In summary, a direct-synthesis approach has been presented here for obtaining GaN nanowires on amorphous substrates with a controllable growth direction. Variation of the Ga flux during the initial stages of nitridation allows for selective growth along the <0001> or <10–10> direction. Homoepitaxial growth onto the nanowires results in different growth modes and morphologies depending upon the nanowire direction: homoepitaxial growth on nanowires grown along the *c*-direction results in hexagonal prism-like islands, while for nanowires grown in the *a*-direction, ribbon-shaped morphologies are obtained. The island growth observed for GaN nanowires grown along the *c*-direction indicates that the surface transport of adatoms on non-polar surfaces occurs via "ballistic" or 1D transport with mean distances exceeding several tens of micrometers.

Experimental

Two types of nitridation experiments were performed: i) direct nitridation of molten Ga droplets using disassociated ammonia, and ii) vapor transport of Ga in dissociated ammonia. The nitridation experiments were performed in an 8 inch (1 inch = 2.54 cm) water-cooled, double-walled, stainless-steel vacuum chamber. Amorphous quartz substrates were used throughout the present study. In the direct nitridation experiments, the quartz substrates were coated with a thin Ga film (approximately 20 μm thick) and placed on a 4 in SiC susceptor that was radiatively heated from the bottom using a tungsten coil filament. The nitridation was performed by exposing the Ga-covered quartz substrates directly to 50 standard cubic centimeters per minute (sccm) of ammonia at 20 torr and 830 °C (1 torr = 133 Pa). The reactive-vapor transport experiments were conducted using pre-synthesized polycrystalline GaN powder as the Ga source. The source was placed on the SiC susceptor and the substrate was placed 2 mm from the Ga source. The substrate temperature was ramped up to 700 °C, and then the flow of NH_3 was initiated while continuing to ramp the temperature to 900 °C in 10 min. The substrates were kept at 20 torr and 900 °C for 1–2 h. The shutdown procedure included lowering the substrate temperature to 700 °C in 10 min, followed by replacing the NH_3 flow with N_2. Finally, the substrate was cooled to room temperature under flowing nitrogen. The homoepitaxial experiments were performed using the same setup and similar conditions as reactive-vapor transport, except that substrates with pre-synthesized GaN nanowires were used. In all cases, the temperature was measured using a c-type thermocouple, which had been calibrated earlier using aluminum (melting point of 660 °C) and germanium (melting point of 937 °C).

Received: August 17, 2005
Published online: December 8, 2005

[1] S. N. Mohammad, A. A. Salvador, H. Morkoc, *Proc. IEEE* **1995**, *83*, 1306.
[2] M. A. Khan, M. S. Shur, *Mater. Sci. Eng., B* **1997**, *46*, 69.
[3] R. F. Davis, S. Einfeldt, E. A. Preble, A. M. Roskowski, Z. J. Reitmeier, P. Q. Miraglia, *Acta Mater.* **2003**, *51*, 5961.
[4] Y. Huang, X. F. Duan, Y. Cui, C. M. Lieber, *Nano Lett.* **2002**, *2*, 101.
[5] J. C. Johnson, H. J. Choi, K. P. Knutsen, R. D. Schaller, P. D. Yang, R. J. Saykally, *Nat. Mater.* **2002**, *1*, 106.
[6] D. P. Feng, Y. Zhao, G. Y. Zhang, *Phys. Status Solidi A* **1999**, *176*, 1003.
[7] P. Waltereit, O. Brandt, A. Trampert, H. T. Grahn, J. Menniger, M. Ramsteiner, M. Reiche, K. H. Ploog, *Nature* **2000**, *406*, 865.
[8] T. Kuykendall, P. J. Pauzauskie, Y. F. Zhang, J. Goldberger, D. Sirbuly, J. Denlinger, P. D. Yang, *Nat. Mater.* **2004**, *3*, 524.
[9] W. S. Shi, Y. F. Zheng, N. Wang, C. S. Lee, S. T. Lee, *Chem. Phys. Lett.* **2001**, *345*, 377.
[10] H. Chandrasekaran, M. K. Sunkara, *Mater. Res. Soc. Symp. Proc.* **2002**, *693*, 159.
[11] M. K. Sunkara, S. Sharma, R. Miranda, G. Lian, E. C. Dickey, *Appl. Phys. Lett.* **2001**, *79*, 1546.
[12] H. Li, H. Chandrasekaran, M. K. Sunkara, R. Collazo, Z. Sitar, M. Stukowski, K. Rajan, *Mater. Res. Soc. Symp. Proc.* **2005**, *831*, E11.34.
[13] S. Vaddiraju, A. Mohite, A. Chin, M. Meyyappan, G. Sumanasekera, B. W. Alphenaar, M. K. Sunkara, *Nano Lett.* **2005**, *5*, 1625.
[14] L. Bergman, X. B. Chen, J. L. Morrison, J. Huso, A. P. Purdy, *J. Appl. Phys.* **2004**, *96*, 675.
[15] I. M. Tiginyanu, V. V. Ursaki, V. V. Zalamai, S. Langa, S. Hubbard, D. Pavlidis, H. Föll, *Appl. Phys. Lett.* **2003**, *83*, 1551.
[16] J. L. Rouviere, M. Arlery, R. Neibuhr, K. H. Bachem, O. Briot, *MRS Internet J. Nitride Semicond. Res.* **1996**, *1*, 33.
[17] D. Moore, C. Ronning, C. Ma, Z. L. Wang, *Chem. Phys. Lett.* **2004**, *385*, 8.
[18] C. Y. Nam, D. Tham, J. E. Fischer, *Appl. Phys. Lett.* **2004**, *85*, 5676.
[19] E. S. Greiner, J. A. Gutowski, W. C. Ellis, *J. Appl. Phys.* **1961**, *32*, 2489.
[20] J. K. Jian, X. L. Chen, M. He, W. J. Wang, X. N. Zhang, F. Shen, *Chem. Phys. Lett.* **2003**, *368*, 416.
[21] G. Deng, A. Ding, W. Cheng, X. Zheng, P. Qiu, *Solid State Commun.* **2005**, *134*, 283.
[22] D. D. Koleske, A. E. Wickenden, R. L. Henry, W. J. DeSisto, R. J. Gorman, *J. Appl. Phys.* **1998**, *84*, 1998.
[23] L. E. Jensen, M. T. Bjork, S. Jeppesen, A. I. Persson, B. J. Ohlsson, L. Samuelson, *Nano Lett.* **2004**, *4*, 1961.
[24] V. T. Binh, P. Melinon, *Surf. Sci.* **1985**, *161*, 234.

